

Galactic cosmic-ray model in the light of AMS-02 nuclei data

Jia-Shu Niu^{1,2,*} and Tianjun Li^{1,2,†}

¹*CAS Key Laboratory of Theoretical Physics, Institute of Theoretical Physics,
Chinese Academy of Sciences, Beijing, 100190, China*

²*School of Physical Sciences, University of Chinese Academy of Sciences, No. 19A Yuquan Road, Beijing 100049, China*
(Dated: December 14, 2024)

Cosmic ray (CR) physics has entered a data-driven era. With the latest AMS-02 nucleus data (boron-to-carbon ratio, proton flux, helium flux and antiproton-to-proton ratio), we perform a global fitting and constrain the primary source and propagation parameters of cosmic rays in the Milky Way by considering the best models (diffusion-reacceleration and diffusion-reacceleration-convection models). We find that this data set can remove the degeneracy between the propagation parameters effectively. The separated injection spectrum parameters are used for proton and other nuclei species, which reveal the different breaks and slopes among them. Moreover, the helium abundance, antiproton production cross sections and solar modulation are parametrized in our global fitting. Benefited from the self-consistence of the new data set, the fitting results show a little bias, and thus the disadvantages and limitations of the existed propagation models appear. It turns out that the problem seems to be more complicated than what we expected based on the previous rough measurements, especially when $E \lesssim 10$ GeV. More interestingly, we obtain some model independent parameters which can provide us some hints to understand the physical meanings or reasons behind them.

I. INTRODUCTION

Galactic cosmic rays (CRs) carry abundant information about its sources and the propagation environments, which provide us a useful tool to probe the properties of the structure of the galaxy, the interstellar medium (ISM) and even dark matter (DM) in the galaxy. During the propagation, the spatial information of CRs' source lost because of the charged CRs diffusive propagation the turbulence of stochastic magnetic field in the galaxy, and they experience possibly the reacceleration, convection, spallation, and energy loss processes [1]. As a result, the propagation of CRs in the Milky Way becomes a fundamental theme to understand the origin and interactions of galactic CRs.

The propagation process can be described by the diffusive transport equation [1]. Based on different simplifications, the transport equation can be solved analytically [2–5]. Alternatively, some numerical packages developed to include most of the relevant processes and the observation-based astrophysical inputs to solve the propagation equation in a self-consistent way, e.g., GALPROP [6], DRAGON [7] and PICARD [8]. Based on these numerical codes, we could set the relevant parameters of the propagation model and get the results according to calculation. These results can be compared with the observational data, and improve the propagation parameters inversely.

The propagation of CRs couples closely with the source, leading to the entanglement between source parameters and propagation parameters. Fortunately, the

secondary-to-primary ratios of nuclei are almost independent of the source injection spectrum. They are always employed to constrain the propagation parameters in Eq. (1). Generally used are the Boron-to-Carbon ratio (B/C) and unstable-to-stable Beryllium ratio ($^{10}\text{Be}/^9\text{Be}$) (see, e.g., [9–12]). But the $^{10}\text{Be}/^9\text{Be}$ data are always with large uncertainties and from different experiment, which always bring large systematics into the subsequent fitting. Recently, Jin et al. [13], Korsmeier and Cuoco [14] claimed that the propagation parameters and the primary sources can be determined using the data of B/C ratio and the proton flux simultaneously. The famous degeneracy between z_h and D_0 can be lifted to some extent in this scenario, which is seriously depend on the precision of the data.

The space station experiment Alpha Magnetic Spectrometer (AMS-02), which was launched in May 2011, improve the measurement precision of the CR fluxes by an order of the systematics [15]. With the results of AMS-02, we could study the CR physics more quantitatively than qualitatively [11, 13, 16–19]. The AMS-02 collaboration has already released its nucleus data for proton [20], helium [21], B/C [22], \bar{p}/p and \bar{p} [23], which provide us the opportunity to study the primary source and propagation models effectively and precisely.

Considering the situations of high-dimensional parameter space of propagation model and precise data sets, we employ a Markov Chain Monte Carlo (MCMC [24]) method (embed by GALPROP) to do global fitting and sample the parameter space of CR propagation and nuclei injections [11, 12, 25]. In this work, we use the AMS-02 nuclei data only, to study the so far 2 best performed propagation models. Specifically, the propagation models include the diffusion-reacceleration (DR) model [9, 10] and the diffusion-reacceleration-convection (DRC) model [12]. Thus the systematics between different experiments

* jsniu@itp.ac.cn

† tli@itp.ac.cn

are avoided and the consistency of the treatment of solar modulation is hold. Additionally, because of the significant difference in the slopes of proton and helium, of about ~ 0.1 [20, 21, 26], has been observed, we use separate primary source spectra settings for proton and other nuclei.

The paper is organized as follows. We first introduce the theoretical aspects on the propagation of CRs in the Galaxy in Sec. II. The fitting procedure is give in Sec. III. After analysis the fitting results in Sec. IV, we make some conclusions and discussions are give in Sec. V.

II. THEORY

Galactic CR particles diffuse in the Galaxy after being accelerated, experiencing the fragmentation and energy loss in the ISM and/or the interstellar radiation field (ISRF) and magnetic field, as well as decay and possible reacceleration or convection. Denoting the density of CRs per unit momentum interval as ψ (which is related to the phase space density $f(\mathbf{r}, \mathbf{p}, t)$ as $\psi(\mathbf{r}, p, t) = 4\pi p^2 f(\mathbf{r}, \mathbf{p}, t)$), the propagation can be described by the propagation equation [1]

$$\frac{\partial \psi}{\partial t} = Q(\mathbf{r}, p) + \nabla \cdot (D_{xx} \nabla \psi - \mathbf{V}_c \psi) + \frac{\partial}{\partial p} p^2 D_{pp} \frac{\partial}{\partial p} \frac{1}{p^2} \psi - \frac{\partial}{\partial p} \left[\dot{p} \psi - \frac{p}{3} (\nabla \cdot \mathbf{V}_c \psi) \right] - \frac{\psi}{\tau_f} - \frac{\psi}{\tau_r}, \quad (1)$$

where $Q(\mathbf{r}, p)$ is the source distribution, D_{xx} is the spatial diffusion coefficient, \mathbf{V}_c is the convection velocity, D_{pp} is diffusion coefficient in the momentum-space, τ_f and τ_r are the characteristic time scales used to describe the fragmentation and radioactive decay.

The convection velocity \mathbf{V}_c is generally assumed to linearly depend on the distance away from the Galaxy disk, $\mathbf{V}_c = \mathbf{z} \cdot dV_c/dz$, where \mathbf{z} is the position vector in the vertical direction to the galactic disk. Such a configuration can avoid the discontinuity at the galactic plane.

The diffusion coefficient can be parameterized as

$$D_{xx} = D_0 \beta (R/R_0)^\delta, \quad (2)$$

where β is the velocity of the particle in unit of light speed c , R_0 is the reference rigidity, and $R \equiv pc/Ze$ is the rigidity.

The reacceleration effect is always used to describe with the diffusion in momentum space. Considering the scenario in which the CR particles are reaccelerated by colliding with the interstellar random weak hydrodynamic waves, the relation between the spatial diffusion coefficient D_{xx} and the momentum diffusion coefficient D_{pp} can be expressed as [27]

$$D_{pp} D_{xx} = \frac{4p^2 v_A^2}{3\delta(4 - \delta^2)(4 - \delta)\omega}, \quad (3)$$

where v_A is the Alfvén velocity and the parameter ω is used to characterize the level of the interstellar turbulence. Because only v_A^2/ω plays a role, we adopt $\omega = 1$ and use v_A to characterize the reacceleration. Free escape is assumed at boundaries, r_h and z_h , for the cylindrical coordinate system.

The injection spectra of all kinds of nuclei are assumed to be a broken power law form

$$q_i(p) = N_i \times \begin{cases} \left(\frac{R}{R_A} \right)^{-\nu_{A1}} & R \leq R_A \\ \left(\frac{R}{R_A} \right)^{-\nu_{A2}} & R > R_A \end{cases}, \quad (4)$$

where i denotes the species of nuclei, N_i is the normalization constant proportional to the relative abundance of the corresponding nuclei, and $\nu_A = \nu_{A1}(\nu_{A2})$ for the nucleus rigidity R below (above) a reference rigidity R_A . In this work, we use independent proton injection spectrum, and the corresponding parameters are R_p , ν_{p1} and ν_{p2} .

The radial distribution of the source term can be determined by independent observables. Based on the distribution of SNR, the spatial distribution of the primary sources is assumed to have the following form [28]

$$f(r, z) = q_0 \left(\frac{r}{r_\odot} \right)^a \exp \left[-b \cdot \frac{r - r_\odot}{r_\odot} - \frac{|z|}{|z_s|} \right], \quad (5)$$

where $a = 1.25$ and $b = 3.56$ are adapted to reproduce the Fermi-LAT gamma-ray data of the 2nd Galactic quadrant [6, 9, 29], $z_s \approx 0.2$ kpc is the characteristic height of Galactic disk, and q_0 is a normalization parameter. In the 2D diffusion model, one can use the realistic non-uniform interstellar gas distribution of $\text{H}_{\text{I,II}}$ and H_2 determined from 21cm and CO surveys. Thus, the injection source function for a specific CR species can be written as follows

$$Q(\mathbf{r}, p) = f(r, z) \cdot q_i(p). \quad (6)$$

The secondary cosmic-ray particles are produced in collisions of primary cosmic-ray particles with ISM. And the secondary antiprotons are generated dominantly from inelastic pp -collisions and $p\text{He}$ -collisions. The corresponding source term is

$$q(\bar{p}) = \beta c n_i \sum_{i=\text{H,He}} \int dp' \frac{\sigma_i(p, p')}{dp'} n_p(p') \quad (7)$$

where n_i is the number density of interstellar hydrogen (helium), n_p is the number density of primary cosmic-ray proton per total momentum, and $d\sigma_i(p, p')/dp'$ is the differential cross section for $p + \text{H(He)} \rightarrow \bar{p} + X$. In our work, we also take into account the production of tertiary antiprotons [30]. Because there are uncertainties from the antiproton production cross section [31–34], we employ an energy-independent factor $c_{\bar{p}}$, which has

been suggested to approximate the ratio of antineutron-to-antiproton production cross sections [34], to rescale the antiproton flux. The energy dependence of $c_{\bar{p}}$ is unclear at present [33, 34]. We expect that a constant factor is a simple and reasonable assumption.

The interstellar flux of the cosmic-ray particle is related to its density function as

$$\Phi = \frac{v}{4\pi} \psi(\mathbf{r}, p). \quad (8)$$

For high energy nuclei $v \approx c$. We adopt the force-field approximation [35] to describe the effects of solar wind and heliospheric magnetic field in the solar system, which contains only one parameter the so-called solar-modulation ϕ . In this approach, the cosmic-ray nuclei flux at the top of the atmosphere of the Earth which is observed by the experiments Φ_{obs} is related to the interstellar flux as follows

$$\Phi_{\text{obs}}(E_{\text{obs}}) = \left(\frac{2mE_{\text{obs}} + E_{\text{obs}}^2}{2mE_{\text{kin}} + E_{\text{kin}}^2} \right) \Phi(E_{\text{kin}}), \quad (9)$$

where $E_{\text{obs}} = E_{\text{kin}} - |Z|e\phi$ is the kinetic energy of the cosmic-ray nuclei measured by the experiments, where Z is the charge number of the cosmic ray particles.

The public code GALPROP v54¹ r2766² [6, 30, 36–38] was used to solve the diffusion equation of Eq. (1) numerically. GALPROP utilizes the realistic astronomical information on the distribution of interstellar gas and other data as input, and considers various kinds of data including primary and secondary nuclei, electrons and positrons, γ -rays, synchrotron radiation, etc, in a self-consistent way. Other approaches based on simplified assumptions on the Galactic gas distribution which allow for fast analytic solutions can be found in Refs. [39–43]. Some custom modifications are performed in the original code, such as the possibility to use specie-dependent injection spectra, which is not allowed by default in GALPROP.

The GALPROP primary source (injection) isotopic abundances are taken first as the solar system abundances, which are iterated to achieve an agreement with the propagated abundances as provided by ACE at ~ 200 MeV/nucleon [44, 45] assuming a propagation model. The source abundances derived for two propagation models, diffusive reacceleration and plain diffusion, were used in many GALPROP runs. In view of some discrepancies when fitting with the new data which use the default abundance in GALPROP [10], we use a factor c_{He} to rescale the helium-4 abundance (which has a default value of 7.199×10^4) which help us to get a global best fitting.

III. FITTING PROCEDURE

A. Bayesian Inference

The Bayesian inference is often used to calculate the posterior probability distribution function (PDF) of the free parameter set $\boldsymbol{\theta} = \{\theta_1, \dots, \theta_m\}$ in a given model, which in fact updates our knowledge from the prior PDF of $\boldsymbol{\theta}$ after taking into account the information provided by the experimental data set D . The relation between the posterior PDF and prior PDF in Bayes' theorem can be expressed as follows

$$p(\boldsymbol{\theta}|D) = \frac{\mathcal{L}(D|\boldsymbol{\theta})\pi(\boldsymbol{\theta})}{p(D)}, \quad (10)$$

where $\mathcal{L}(D|\boldsymbol{\theta})$ is the likelihood function, and $\pi(\boldsymbol{\theta})$ is the prior PDF which represents our state of knowledge on the values of the parameters before taking into account of the new data. The quantity $p(D)$ is the Bayesian evidence which is obtained by integrating the product of the likelihood and the prior over the whole volume of the parameter space

$$p(D) = \int_V \mathcal{L}(D|\boldsymbol{\theta})\pi(\boldsymbol{\theta})d\boldsymbol{\theta}. \quad (11)$$

This quantity is important for Bayesian model comparison. It is straight forward to obtain the marginal PDFs of interested parameters $\{\theta_1, \dots, \theta_n\} (n < m)$ by integrating out other nuisance parameters $\{\theta_{n+1}, \dots, \theta_m\}$

$$p(\theta_1, \dots, \theta_n)_{\text{marg}} = \int p(\boldsymbol{\theta}|D) d\theta_{n+1} \dots d\theta_m. \quad (12)$$

The marginal PDF is often used in visual presentation. If there is no preferred value of θ_i in the allowed range $(\theta_{i,\text{min}}, \theta_{i,\text{max}})$, the priors can be taken as a uniform distribution

$$\pi(\theta_i) \propto \begin{cases} 1, & \text{for } \theta_{i,\text{min}} < \theta_i < \theta_{i,\text{max}} \\ 0, & \text{otherwise} \end{cases}. \quad (13)$$

The likelihood function is often assumed to be a Gaussian form

$$\mathcal{L}(D|\boldsymbol{\theta}) = \prod_i \frac{1}{\sqrt{2\pi\sigma_i^2}} \exp \left[-\frac{(f_{\text{th},i}(\boldsymbol{\theta}) - f_{\text{exp},i})^2}{2\sigma_i^2} \right], \quad (14)$$

where $f_{\text{th},i}(\boldsymbol{\theta})$ is the predicted i -th observable from the model which depends on the parameter set $\boldsymbol{\theta}$, and $f_{\text{exp},i}$ is the one measured by the experiment with uncertainty σ_i . When the form of the likelihood function is confirmed, the posterior PDF can be determined by sampling the distribution from the prior PDF using the Markov Chain Monte Carlo (MCMC) methods.

Here we use the algorithms such as the one by Goodman and Weare [46] instead of classical Metropolis-Hastings for its excellent performance on clusters. The

¹ <http://galprop.stanford.edu>

² <https://sourceforge.net/projects/galprop/>

algorithm by Goodman and Weare [46] was slightly altered and implemented as the Python module `emcee`³ by Foreman-Mackey et al. [47], which makes it easy to use by the advantages of Python. Moreover, `emcee` could distribute the sampling on the multiple nodes of modern cluster or cloud computing environments, and then increase the sampling efficiency observably.

The posterior statistic mean value of the parameter θ_i can be obtained from the posterior PDF $P(\theta|D)$ in a straightforward way. Using the MCMC sequence $\{\theta_i^{(1)}, \theta_i^{(2)}, \dots, \theta_i^{(N)}\}$ (after burn-in) of the parameter θ_i with N the length of the Markov chain, the mean (expectation) value $\langle\theta_i\rangle$ is given by

$$\langle\theta_i\rangle = \int \theta_i P(\theta_i|D) d\theta_i = \frac{1}{N} \sum_{k=1}^N \theta_i^{(k)}, \quad (15)$$

and the standard deviation of the parameters θ_i is given by $\sigma^2 = \sum_{k=1}^N (\theta_i^{(k)} - \langle\theta_i\rangle)^2 / (N - 1)$.

B. Data Sets

In our work, we propose a scheme which utilizes the proton [20], helium [21], B/C [22] and \bar{p}/p [23] AMS-02 data together to determine the primary source and propagation parameters. The benefits are as follows: (i): the statistics of the AMS-02 data on charged cosmic-ray particles are now much higher than the other experiments and will continue to increase; (ii) these data can constitute a complete data sets to determine the related parameters; (iii) this scheme can avoid the complications involving the combination of the systematics of different type of experiments; (iv) this scheme can estimate the effect of solar modulation consistently; (v) this scheme fit the proton and helium data simultaneously and do the subsequent fitting of positron and electron (whose secondary species are primarily generated by proton and helium) in a self-consistent way.

C. Parameters for Different Models

In this work, the whole data is

$$D = \{D_p^{\text{AMS}}, D_{He}^{\text{AMS}}, D_{B/C}^{\text{AMS}}, D_{\bar{p}/p}^{\text{AMS}}\}^4. \quad (16)$$

For DR model, the convection velocity $\mathbf{V}_c = 0$. We consider the case $R = 20$ kpc and spatial independent diffusion coefficient. Thus, the major parameters to describe the propagation are (D_0, δ, v_A, z_h) .

The primary source term can be determined by Eq. (6), from which we get free parameters: the power-law indices ν_{p1} and ν_{p2} (for proton), as well as ν_{A1} and ν_{A2} (for other nuclei); the break in rigidity R_p and R_A ; the normalization factor N_p at a reference kinetic energy $E_{kin} = 100$ GeV; the solar modulation is described by ϕ . Additionally, as described in Sec. II, we employ a factor c_{He} to rescale the isotopic abundance of helium [10, 14] and a factor $c_{\bar{p}}$ to rescale the calculated secondary flux to fit the data (which in fact account for the antineutron-to-antiproton production ratio [34, 48]).

The radial and z grid steps are chosen as $\Delta r = 1$ kpc, and $\Delta z = 0.2$ kpc. The grid in kinetic energy per nucleon is logarithmic between 10^2 and 10^7 MeV with a step factor of 1.2. The free escape boundary conditions are used by imposing ψ equal to zero outside the region sampled by the grid.

Altogether, we have 14 free parameters for DR model

$$\theta = \{D_0, \delta, z_h, v_A, |N_p, R_p, \nu_{p1}, \nu_{p2}, R_A, \nu_{A1}, \nu_{A2}, |c_{He}, c_{\bar{p}}, \phi\}. \quad (17)$$

We add dv/dz into Eq. (17) and then have 15 free parameters for DRC model

$$\theta = \{D_0, \delta, z_h, v_A, dv/dz, |N_p, R_p, \nu_{p1}, \nu_{p2}, R_A, \nu_{A1}, \nu_{A2}, |c_{He}, c_{\bar{p}}, \phi\}. \quad (18)$$

These parameters can be separated into three groups: the propagation parameters, the source parameters and nuisance parameters. And their priors are chosen to be uniform distributions according to Eq. (13) with the prior intervals given in Tables I and II.

IV. FITTING RESULTS

We use the MCMC algorithm to determine the model parameters of the three models as described in Sec. III through fitting to the data set. When the Markov Chains have reached their equilibrium state we take the samples of the parameters as their posterior PDFs. The best-fitting results and the corresponding residuals of the spectra and ratios are showed in Fig. 1 (B/C), Fig. 2 (proton and helium) and Fig. 3 (antiproton). The best-fit values, statistical mean values, standard deviations and allowed intervals at 95% CL for these parameters are shown in Tab. I (for DR model) and Tab. II (for DRC model). The DRC model fits the data slightly better than DR model in low-energy regions because of the additional parameter dv/dz .

Because the data are precise enough and from the same experiment at the same period, we obtain statistically the good constraints on the model parameters. Some of the model parameters, such as the injection spectral indices, are constrained to a level of $\lesssim 1\%$. The propagation parameters are constrained to be about $\lesssim 10\%$, which are relatively large due to the degeneracy among some of them but obtained an obvious improvement compared

³ <http://dan.iel.fm/emcee/>

⁴ Considering the degeneracy between $D_{\bar{p}/p}^{\text{AMS}}$ and D_p^{AMS} , we just use $D_{\bar{p}/p}^{\text{AMS}}$ to do MCMC fitting and use them together to show the fitting result.

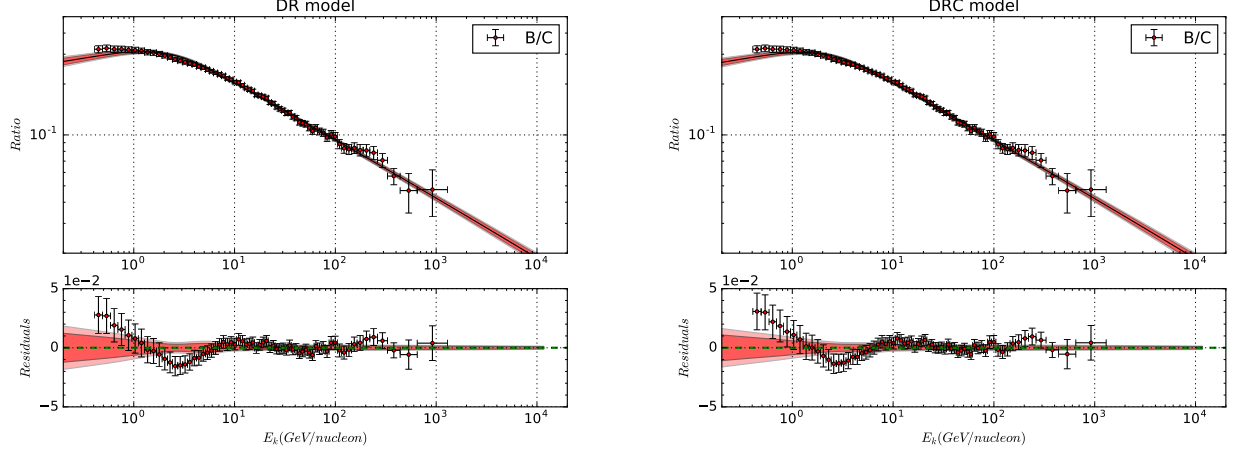


FIG. 1: The global fitting results and the corresponding residuals to the AMS-02 B/C ratio data for DR and DRC model. The 2σ (deep red) and 3σ (light red) bound are also showed in the figures.

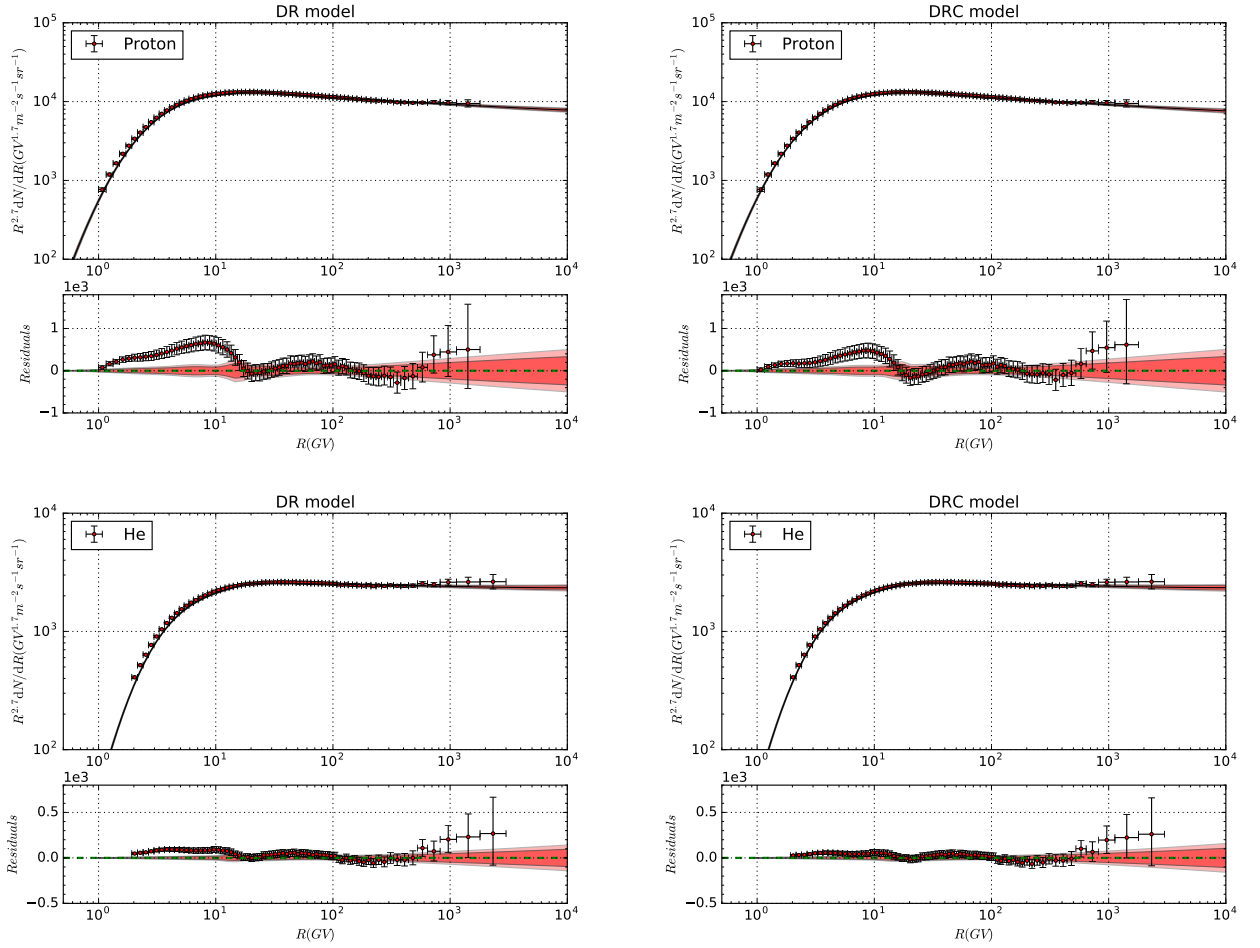


FIG. 2: The global fitting results and the corresponding residuals to the AMS-02 proton and helium flux data for DR and DRC model. The 2σ (deep red) and 3σ (light red) bound are also showed in the figures.

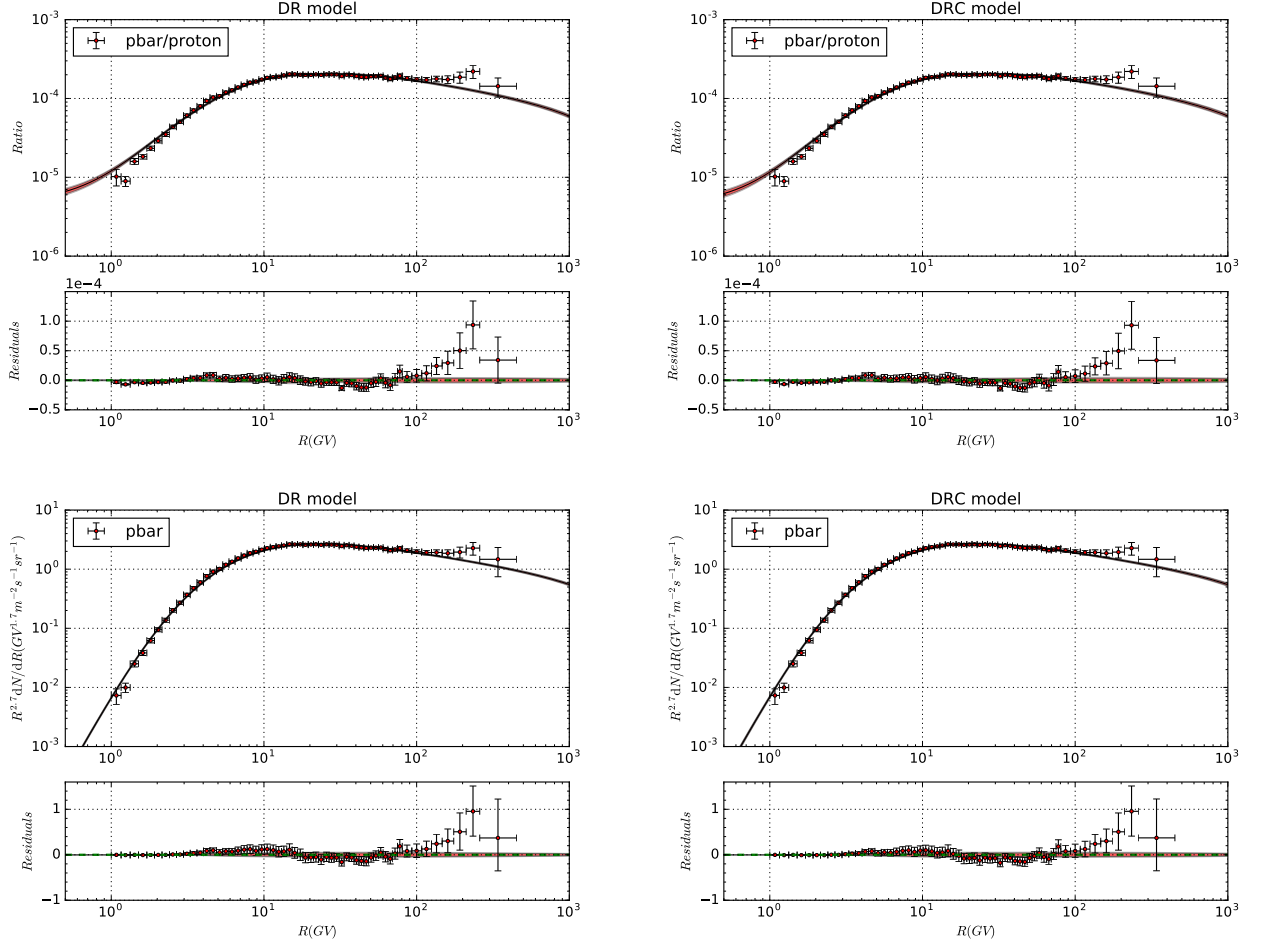


FIG. 3: The global fitting results and the corresponding residuals to the AMS-02 \bar{p}/p ratio and \bar{p} flux data for DR and DRC model. The 2σ (deep red) and 3σ (light red) bound are also showed in the figures. Note that the \bar{p} data is not used in the global fitting and we show it for a cross validation.

with previous studies [9–14]. For the rigidity-dependent slope of the diffusion coefficient, δ , the statistical error is only a few percent ($\lesssim 2\%$). The uncertainties of three nuisance parameters are $\lesssim 10\%$, which give us an opportunity to read the relevant information behind these parameters.

For a comparison, we also present the posterior mean and 68% credible uncertainties determined from a previous analysis in Yuan et al. [12] and which is based on data of B/C (from AMS-02 [22] and ACE-CRIS ⁵), $^{10}\text{Be}/^9\text{Be}$ (from Ulysses [49], ACE [50], Voyager [51], IMP [52], ISEE-3 [52], and ISOMAX [53]) and proton flux (from AMS-02 [20] and PAMELA [54]) for DR and DRC models.

The major discrepancy comes from the fitting results of B/C ratio (Fig. 1), proton and helium flux (Fig. 2) below ~ 10 GeV, and \bar{p}/p ratio and \bar{p} flux (Fig. 3)

larger than ~ 100 GeV. The first may be because the propagations of heavy nuclei like B and C are different from the propagations of light nuclei like p and \bar{p} [10] (see also [12, 55, 56]) and the limitation of the force-field approximation to describe the CR properties within the effects of solar wind and heliospheric magnetic field in the solar system. The second is more interesting and might be interpreted as dark matter annihilation [48, 57].

In consideration of the relatively independent among three groups of the models' parameters (the propagation parameters, the source parameters and nuisance parameters), we would analyze the results of these three groups separately. At the same time, we compare the different aspects of these two models.

A. Propagation Parameters

The results of posterior probability distributions of the propagation parameters are shown in Fig. 4 (DR model)

⁵ <http://www.srl.caltech.edu/ACE/ASC/level2/lvl2DATA-CRIS.html>

ID	Prior range	Best-fit value	Posterior mean and Standard deviation	Posterior 95% range	Ref. Yuan et al. [12]
D_0 ($10^{28} \text{ cm}^2 \text{ s}^{-1}$)	[1, 12]	9.97	8.81 ± 0.72	[8.03, 10.48]	7.24 ± 0.97
δ	[0.1, 1.0]	0.376	0.376 ± 0.009	[0.366, 0.380]	0.380 ± 0.007
z_h (kpc)	[0.5, 20.0]	9.12	7.37 ± 0.62	[6.22, 9.37]	5.93 ± 1.13
v_A (km/s)	[0, 50]	38.6	38.5 ± 3.2	[37.4, 41.7]	38.5 ± 1.3
N_p^a	[1, 8]	4.44	4.44 ± 0.02	[4.41, 4.46]	4.50 ± 0.02
R_p (GV)	[1, 30]	18.8	17.4 ± 1.9	[16.5, 20.2]	12.9 ± 0.6
ν_{p1}	[1.0, 4.0]	2.004	1.990 ± 0.022	[1.981, 2.028]	1.69 ± 0.02
ν_{p2}	[1.0, 4.0]	2.404	2.409 ± 0.008	[2.400, 2.423]	2.37 ± 0.01
R_A (GV)	[1, 30]	17.9	16.1 ± 1.7	[15.8, 18.8]	12.9 ± 0.6
ν_{A1}	[1.0, 4.0]	2.002	1.985 ± 0.027	[1.979, 2.025]	1.69 ± 0.02
ν_{A2}	[1.0, 4.0]	2.348	2.350 ± 0.006	[2.343, 2.361]	2.37 ± 0.01
c_{He}	[0.1, 5.0]	0.69	0.73 ± 0.07	[0.63, 0.84]	—
c_{pbar}	[0.1, 5.0]	1.34	1.34 ± 0.05	[1.33, 1.39]	—
ϕ (GV)	[0, 1.5]	0.62	0.62 ± 0.03	[0.58, 0.67]	0.86 ± 0.02

^a Post-propagated normalization flux of protons at 100 GeV in unit $10^{-9} \text{ cm}^{-2} \text{ s}^{-1} \text{ sr}^{-1} \text{ MeV}^{-1}$

TABLE I: Constraints on the propagation models from the global Bayesian analyses to the AMS-02 data of B/C ratio, proton, helium flux and \bar{p}/p ratio. The prior interval, best-fit value, statistic mean, standard deviation and the allowed range at 95% CL are listed for each propagation parameter. For a comparison, we also list the posterior mean and 68% credible uncertainties of these parameters from a previous analysis in Yuan et al. [12]. For best-fit values, $\chi^2/d.o.f. = 251.48/248$.

ID	Prior range	Best-fit value	Posterior mean and Standard deviation	Posterior 95% range	Ref. Yuan et al. [12]
D_0 ($10^{28} \text{ cm}^2 \text{ s}^{-1}$)	[1, 12]	10.82	9.70 ± 0.67	[8.62, 11.20]	6.14 ± 0.45
δ	[0.1, 1.0]	0.378	0.376 ± 0.006	[0.368, 0.389]	0.478 ± 0.013
z_h (kpc)	[0.5, 20.0]	11.15	9.05 ± 1.05	[7.57, 11.62]	12.70 ± 1.40
v_A (km/s)	[0, 50]	38.1	40.2 ± 1.3	[37.3, 41.7]	43.2 ± 1.2
dv/dz ($\text{km s}^{-1} \text{ kpc}^{-1}$)	[0, 30]	0.56	2.01 ± 1.31	[0.09, 3.48]	11.99 ± 1.26
N_p^a	[1, 8]	4.42	4.44 ± 0.02	[4.41, 4.46]	4.52 ± 0.02
R_p (GV)	[1, 30]	19.1	18.8 ± 0.9	[18.0, 20.6]	16.6 ± 1.2
ν_{p1}	[1.0, 4.0]	2.015	2.022 ± 0.015	[1.997, 2.047]	1.82 ± 0.02
ν_{p2}	[1.0, 4.0]	2.409	2.416 ± 0.012	[2.403, 2.424]	2.37 ± 0.01
R_A (GV)	[1, 30]	18.4	17.6 ± 0.8	[16.7, 19.4]	16.6 ± 1.2
ν_{A1}	[1.0, 4.0]	2.018	2.020 ± 0.015	[1.998, 2.051]	1.82 ± 0.02
ν_{A2}	[1.0, 4.0]	2.348	2.355 ± 0.009	[2.344, 2.363]	2.37 ± 0.01
c_{He}	[0.1, 5.0]	0.66	0.70 ± 0.07	[0.59, 0.85]	—
c_{pbar}	[0.1, 5.0]	1.37	1.38 ± 0.04	[1.34, 1.40]	—
ϕ (GV)	[0, 1.5]	0.62	0.62 ± 0.02	[0.57, 0.67]	0.89 ± 0.03

^a Post-propagated normalization flux of protons at 100 GeV in unit $10^{-9} \text{ cm}^{-2} \text{ s}^{-1} \text{ sr}^{-1} \text{ MeV}^{-1}$

TABLE II: Same as Table I but for DRC model. Note that add a propagation parameter dv/dz . For best-fit values, $\chi^2/d.o.f. = 246.69/247$.

and Fig. 5 (DRC model). In general, this data set favors large values of D_0 and z_h .

In Fig. 4, there is a clear degeneracy between D_0 and z_h . This is because the B/C data can only constrain D_0/z_h effectively [13, 58]. More importantly, although there still exists the degeneracy between D_0 and z_h , the \bar{p}/p data can effectively relieve the degeneracy of this classical correlation and our results show a concrete improvement compared with previous works (see for e.g., [10, 12, 14]).

In Fig. 5, the degeneracy between D_0 and z_h which is

enlarged by the additional parameter dv/dz . But what is interesting is that the result favors a small value of $dv/dz \sim 0.558 \text{ km/s}$, which is largely different from the result in Yuan et al. [12] ($dv/dz \sim 11.99 \text{ km/s}$). This difference may come from the bias of different experiment and large uncertainties of the $^{10}\text{Be}/^9\text{Be}$ data.

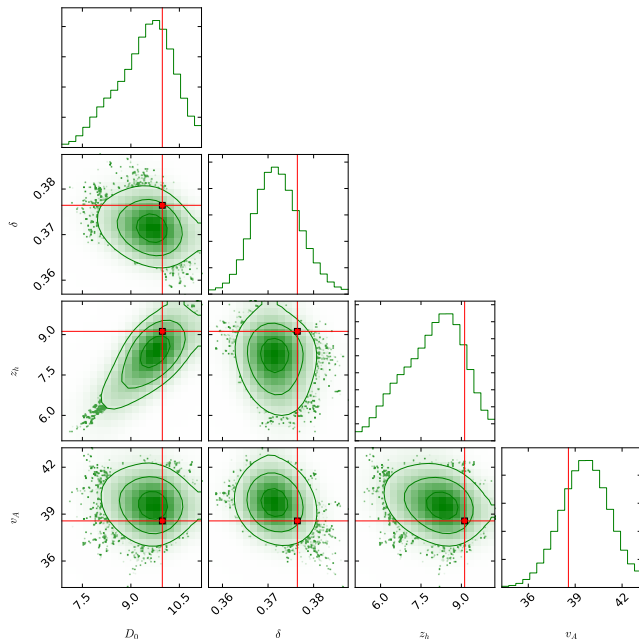


FIG. 4: Fitting 1D probability and 2D credible regions of posterior PDFs for the combinations of all propagation parameters from DR model. The regions enclosing σ , 2σ and 3σ CL are shown in step by step lighter green. The red cross lines and marks in each plot indicates the best-fit value (largest likelihood).

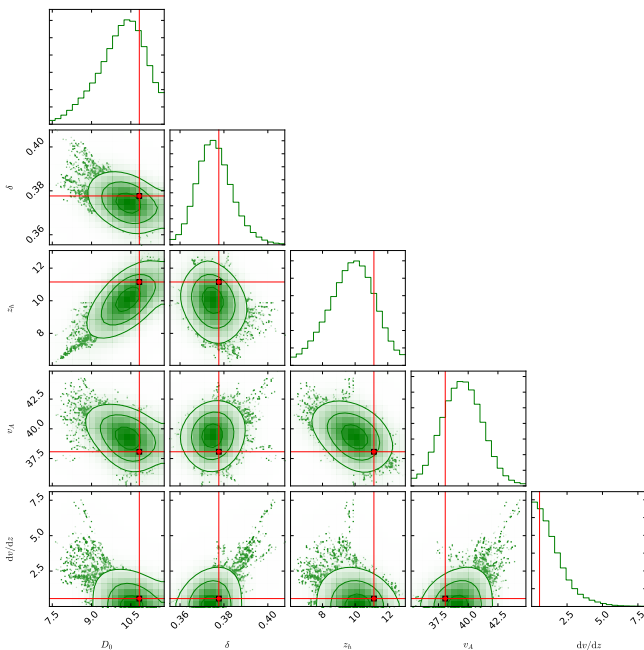


FIG. 5: Same as Fig. 4 but for DRC models.

B. Primary Source Parameters

The results of posterior probability distributions of the primary source parameters are shown in Fig. 6 (DR model) and Fig. 7 (DRC model). Because we do not have obvious correlations in these figures, the posterior PDFs of these parameters are in a high confidence level and provide us the opportunity to study the CR physics behind them.

Benefited from the independent injection spectra for proton and other nuclei, we present the differences between rigidity breaks and slopes for proton and other nuclei species ($R_p - R_A$, $\nu_{p1} - \nu_{A1}$, $\nu_{p2} - \nu_{A2}$) in Fig. 8 and Tab. III. In detail, $R_p - R_A$ and $\nu_{p1} - \nu_{A1}$ has a slight different values for DR and DRC model, but has a relatively large overlap. For $\nu_{p2} - \nu_{A2}$, we have a high confidence level that the value is ~ 0.06 .

ID	DR model	DRC model
$R_p - R_A$	1.30 ± 0.65	1.05 ± 0.81
$\nu_{p1} - \nu_{A1}$	0.0014 ± 0.0063	-0.0020 ± 0.0066
$\nu_{p2} - \nu_{A2}$	0.0600 ± 0.0041	0.060 ± 0.0044

TABLE III: The posterior mean and standard deviation of $R_p - R_A$, $\nu_{p1} - \nu_{A1}$, $\nu_{p2} - \nu_{A2}$ for DR and DRC models.

C. Nuisance Parameters

In Fig. 9, we can see that in DR and DRC models, the nuisance parameters are almost the same. This represent the necessity to introduce them and the relatively independent physics behind them.

In this work, we can see that if we want to fit the AMS-02 helium data in a self-consistent way, the helium-4 abundant should have a factor ~ 0.68 compared to the original value in GALPROP (7.199×10^4). What is more interesting, this value is model independent to some extent which increase the degree of confidence of this result.

The uncertainties on the antiproton production cross sections could produce the relevant uncertainties in the antiproton flux [34, 55], and the employed energy (or rigidity) independent factor $c_{\bar{p}}$ can reproduce the AMS-02 antiproton flux result well except when $R \gtrsim 100$ GV. Considering its model independent property this factor becomes an effective and highly confident value to reproduce the CR background and find new physics [48].

The model independent solar modulation ϕ provide an relatively effective but not that precise fitting of the current data set. Benefited from the precise and self-consistent AMS-02 nuclei data set, the inefficient fitting in low-energy regions of force-field approximation is obviously represented in Figs. 1 and 2. Of course, these discrepancy also may partly come from the different prop-

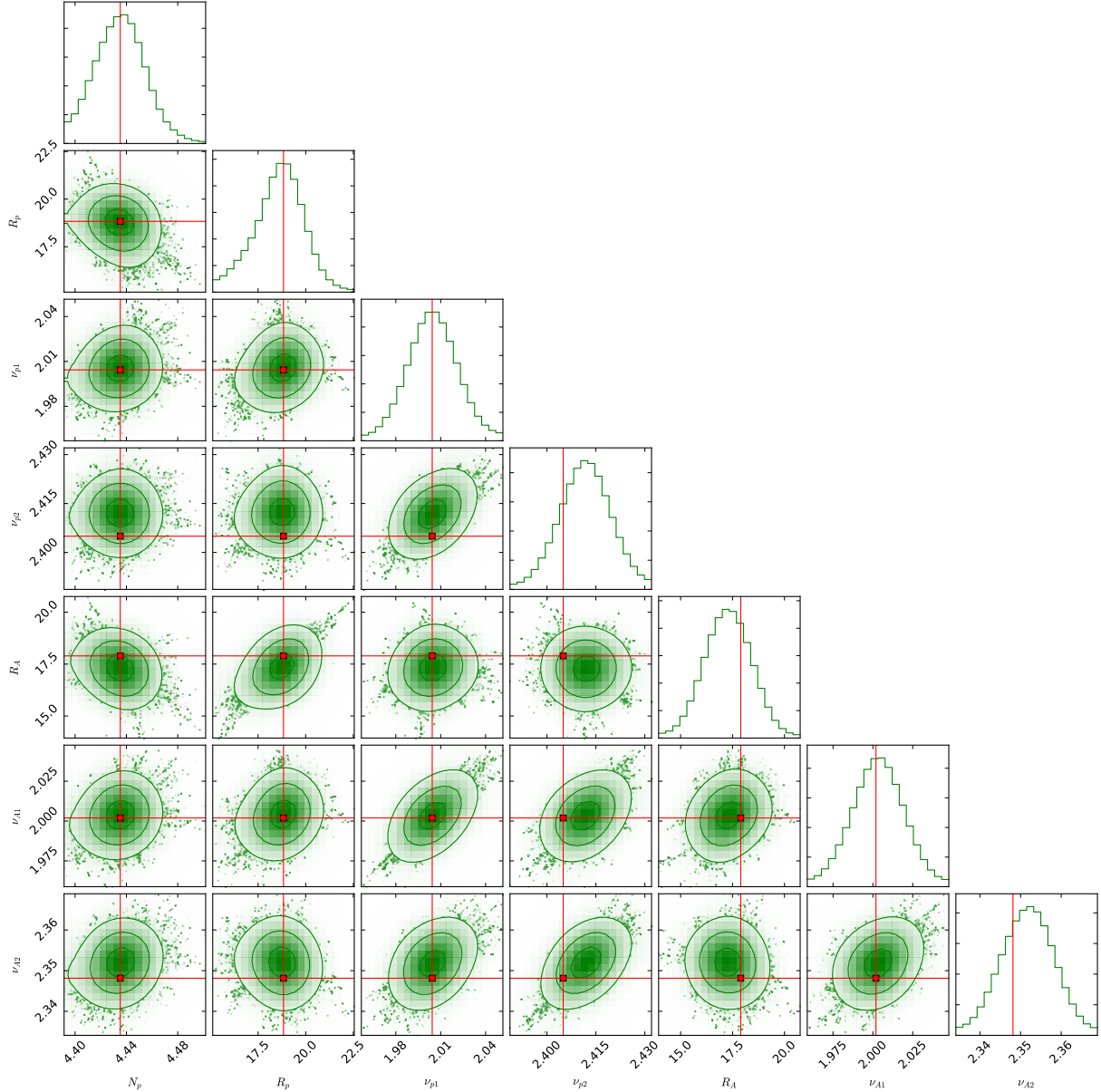


FIG. 6: Fitting 1D probability and 2D credible regions of posterior PDFs for the combinations of primary source parameters from DR model. The regions enclosing σ , 2σ and 3σ CL are shown in step by step lighter green. The red cross lines and marks in each plot indicates the best-fit value (largest likelihood).

agations from heavy elements and light elements [10], which require a deeply subsequent studying on these aspects.

V. DISCUSSIONS AND CONCLUSION

In this work, we use the newly released AMS-02 nucleus data (B/C, proton, helium and \bar{p}/p) only, to study 2 so far best performed propagation models (DR and DRC model). In this scenario, the systematics between

different experiments are avoided and the consistency of the treatment of solar modulation is hold. Additionally, we use separate primary spectra settings for proton and other nucleus because of the observed significant difference in the slopes of proton and helium, which can reveal the sources' differences between them.

According to the fitting results and the posterior PDFs of different groups of the models' parameters, we present our main conclusion as follows.

- (i) The newly reported AMS-02 nuclei data (B/C, proton, helium and \bar{p}/p) can effectively relieve

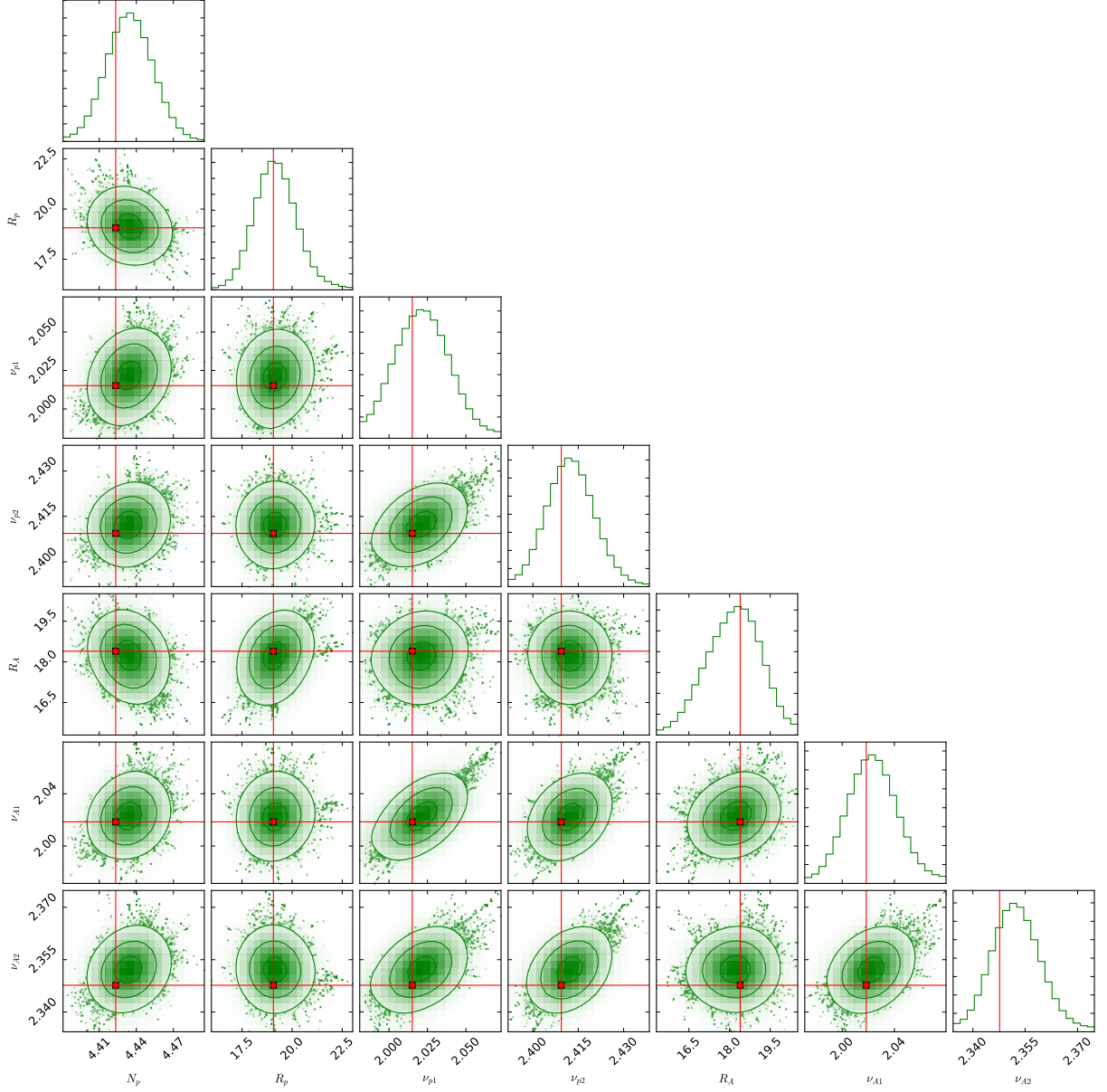


FIG. 7: Same as Fig. 6 but for DRC model.

the degeneracy of the classical correlation between D_0 and z_h , and our results for the constraints on some parameters show a concrete improvement compared with previous works. Benefited from the self-consistence of the new data set from AMS-02, the fitting results (see Figs. 1, 2, and 3) show a little bias (note the 2σ and 3σ bounds), and thus the disadvantages and limitations of the existed propagation models emerge.

- (ii) Based on (i), the major discrepancy comes from the fitting results lower than ~ 10 GeV should come from the propagation models rather than the data. This discrepancy calls for a detailed improvement

to handle the solar modulation and deeply studying the different propagations from heavy elements and light elements in low-energy regions.

- (iii) Also based on (ii), there is an obvious excess for \bar{p} flux and \bar{p}/p ratio data which could not be explained by the standard propagation models. This gives a concrete hint to search for dark matter [48, 57].
- (iv) There exist some model independent parameters which represent the corresponding CR physics behind them. The difference of the injection spectrum break between proton and other nucleus $R_p -$

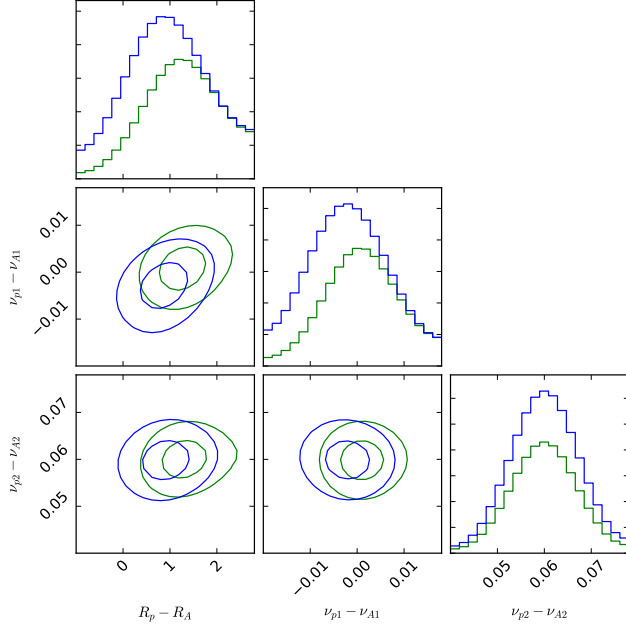


FIG. 8: Fitting 1D probability and 2D credible regions of posterior PDFs for the differences of primary source parameters (green for DR model, blue for DRC model). The regions enclosing σ and 2σ CL are indicated by the contours.

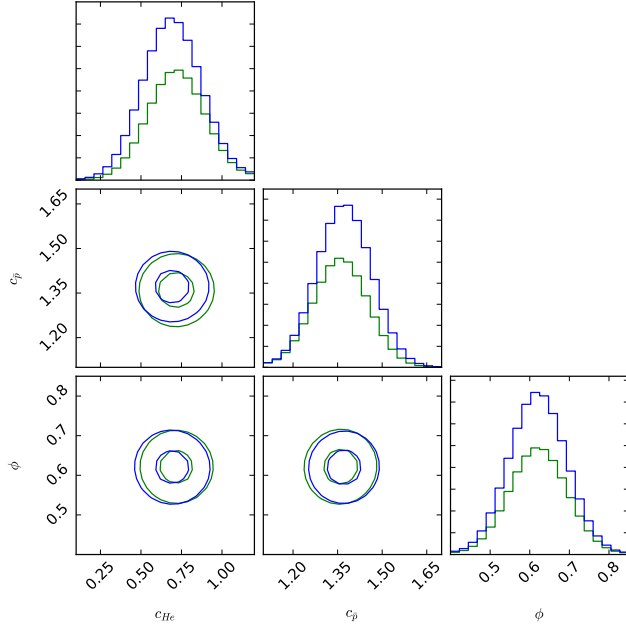


FIG. 9: Fitting 1D probability and 2D credible regions of posterior PDFs for the combinations of nuisance parameters from DR (green lines) and DRC (blue lines) models. The regions enclosing σ and 2σ CL are indicated by the contours.

$R_A \sim 1$ GV, and the second slopes between them $\nu_{p2} - \nu_{A2} \sim 0.06$ which has a high level of confidence and interpret that the primary source of proton is different from other nuclei when $R \gtrsim 18$ GV. Additionally, the helium-4 abundance have a value of $\sim 4.895 \times 10^4 = 0.6868 \times (7.199 \times 10^4)$, the energy-independent rescaling factor $c_{\bar{p}}$ have a value of $1.33 - 1.39$ within a confidence level of 95% and the effective solar modulation $\phi \sim 0.62$.

Thanks to the precise measurements of CR data by AMS-02, with more and more precise data available, we are going into a data-driven era and able to investigate the CR-related problems in great details. With the results of this work, it turns out that the problem seems to be more complicated than what we expected based on the rough measurements in the past (especially in the low-energy region). The model independent parameters provide us hints to reveal the physical meanings or reasons behind them. Thus, CR physics becomes a comprehensive discipline which now requires the improvement not only for itself, but also other disciplines like atomic physics and space physics.

ACKNOWLEDGMENTS

We would like to thank Xiao-Jun Bi, Su-Jie Lin, and Qiang Yuan very much for helpful discussions, Foreman-Mackey [59] to provide us the tool to visualize multidimensional samples using a scatterplot matrix, and Maurin et al. [60] to collect database and associated online tools for charged cosmic-ray measurements. This research was supported in part by the Projects 11475238 and 11647601 supported by National Science Foundation of China, and by Key Research Program of Frontier Sciences, CAS.

-
- [1] A. W. Strong, I. V. Moskalenko, and V. S. Ptuskin, *Annual Review of Nuclear and Particle Science* **57**, 285 (2007), astro-ph/0701517.
- [2] W. R. Webber, M. A. Lee, and M. Gupta, *Astrophys. J.* **390**, 96 (1992).
- [3] J. B. G. M. Bloemen, V. A. Dogiel, V. L. Dorman, and V. S. Ptuskin, *Astron. Astrophys.* **267**, 372 (1993).
- [4] D. Maurin, R. Taillet, and F. Donato, *Astron. Astrophys.* **394**, 1039 (2002), astro-ph/0206286.
- [5] T. Shibata, M. Hareyama, M. Nakazawa, and C. Saito, *Astrophys. J.* **612**, 238 (2004).
- [6] A. W. Strong and I. V. Moskalenko, *Astrophys. J.* **509**, 212 (1998), astro-ph/9807150.
- [7] C. Evoli, D. Gaggero, D. Grasso, and L. Maccone, *J. Cosmol. Astropart. Phys.* **10**, 018 (2008), arXiv:0807.4730.
- [8] R. Kissmann, *Astroparticle Physics* **55**, 37 (2014), arXiv:1401.4035 [astro-ph.HE].
- [9] R. Trotta, G. Jóhannesson, I. V. Moskalenko, T. A. Porter, R. Ruiz de Austri, and A. W. Strong, *Astrophys. J.* **729**, 106 (2011), arXiv:1011.0037 [astro-ph.HE].
- [10] G. Jóhannesson, R. Ruiz de Austri, A. C. Vincent, I. V. Moskalenko, E. Orlando, T. A. Porter, A. W. Strong, R. Trotta, F. Feroz, P. Graff, and M. P. Hobson, *Astrophys. J.* **824**, 16 (2016), arXiv:1602.02243 [astro-ph.HE].
- [11] S.-J. Lin, Q. Yuan, and X.-J. Bi, *Physical Review D* **91**, 063508 (2015), arXiv:1409.6248 [astro-ph.HE].
- [12] Q. Yuan, S.-J. Lin, K. Fang, and X.-J. Bi, *ArXiv e-prints* (2017), arXiv:1701.06149 [astro-ph.HE].
- [13] H.-B. Jin, Y.-L. Wu, and Y.-F. Zhou, *J. Cosmol. Astropart. Phys.* **9**, 049 (2015), arXiv:1410.0171 [hep-ph].
- [14] M. Korsmeier and A. Cuoco, *ArXiv e-prints* (2016), arXiv:1607.06093 [astro-ph.HE].
- [15] AMS Collaboration, M. Aguilar, G. Alberti, B. Alpat, A. Alvino, G. Ambrosi, K. Andeen, H. Anderhub, L. Arruda, P. Azzarello, A. Bachlechner, and et al., *Physical Review Letters* **110**, 141102 (2013).
- [16] H.-B. Jin, Y.-L. Wu, and Y.-F. Zhou, *J. Cosmol. Astropart. Phys.* **11**, 026 (2013), arXiv:1304.1997 [hep-ph].
- [17] L. Feng, R.-Z. Yang, H.-N. He, T.-K. Dong, Y.-Z. Fan, and J. Chang, *Physics Letters B* **728**, 250 (2014), arXiv:1303.0530 [astro-ph.HE].
- [18] M. Di Mauro, F. Donato, N. Fornengo, R. Lineros, and A. Vittino, *J. Cosmol. Astropart. Phys.* **4**, 006 (2014), arXiv:1402.0321 [astro-ph.HE].
- [19] Q. Yuan and X.-J. Bi, *J. Cosmol. Astropart. Phys.* **3**, 033 (2015), arXiv:1408.2424 [astro-ph.HE].
- [20] AMS Collaboration, M. Aguilar, D. Aisa, B. Alpat, A. Alvino, G. Ambrosi, K. Andeen, L. Arruda, N. Attig, P. Azzarello, A. Bachlechner, and et al., *Physical Review Letters* **114**, 171103 (2015).
- [21] AMS Collaboration, M. Aguilar, D. Aisa, B. Alpat, A. Alvino, G. Ambrosi, K. Andeen, L. Arruda, N. Attig, P. Azzarello, A. Bachlechner, and et al., *Physical Review Letters* **115**, 211101 (2015).
- [22] AMS Collaboration, M. Aguilar, L. Ali Cavasonza, G. Ambrosi, L. Arruda, N. Attig, S. Aupetit, P. Azzarello, A. Bachlechner, F. Barao, A. Barrau, and et al., *Phys. Rev. Lett.* **117**, 231102 (2016).
- [23] AMS Collaboration, M. Aguilar, L. Ali Cavasonza, B. Alpat, G. Ambrosi, L. Arruda, N. Attig, S. Aupetit, P. Azzarello, A. Bachlechner, F. Barao, and et al., *Physical Review Letters* **117**, 091103 (2016).
- [24] A. Lewis and S. Bridle, *Phys. Rev. D* **66**, 103511 (2002), astro-ph/0205436.
- [25] J. Liu, Q. Yuan, X. Bi, H. Li, and X. Zhang, *Phys. Rev. D* **81**, 023516 (2010), arXiv:0906.3858 [astro-ph.CO].
- [26] PAMELA Collaboration, O. Adriani, G. C. Barbarino, G. A. Bazilevskaya, R. Bellotti, M. Boezio, E. A. Bogomolov, L. Bonechi, M. Bongi, V. Bonvicini, S. Borisov, and et al., *Science* **332**, 69 (2011), arXiv:1103.4055 [astro-ph.HE].
- [27] E. S. Seo and V. S. Ptuskin, *Astrophys. J.* **431**, 705 (1994).
- [28] G. Case and D. Bhattacharya, *American Association of Pharmaceutical Scientists* **120**, 437 (1996).
- [29] Fermi-LAT Collaboration, L. Tibaldo, and I. A. Grenier, *ArXiv e-prints* (2009), arXiv:0907.0312 [astro-ph.HE].
- [30] I. V. Moskalenko, A. W. Strong, J. F. Ormes, and M. S. Potgieter, *Astrophys. J.* **565**, 280 (2002), astro-ph/0106567.
- [31] L. C. Tan and L. K. Ng, *Journal of Physics G Nuclear Physics* **9**, 1289 (1983).
- [32] R. P. Duperray, C.-Y. Huang, K. V. Protasov, and M. Buénerd, *Phys. Rev. D* **68**, 094017 (2003), astro-ph/0305274.
- [33] R. Kappl and M. W. Winkler, *J. Cosmol. Astropart. Phys.* **9**, 051 (2014), arXiv:1408.0299 [hep-ph].
- [34] M. di Mauro, F. Donato, A. Goudelis, and P. D. Serpico, *Phys. Rev. D* **90**, 085017 (2014), arXiv:1408.0288 [hep-ph].
- [35] L. J. Gleeson and W. I. Axford, *Astrophys. J.* **154**, 1011 (1968).
- [36] A. W. Strong and I. V. Moskalenko, *Advances in Space Research* **27**, 717 (2001), astro-ph/0101068.
- [37] I. V. Moskalenko, A. W. Strong, S. G. Mashnik, and J. F. Ormes, *Astrophys. J.* **586**, 1050 (2003), astro-ph/0210480.
- [38] V. S. Ptuskin, I. V. Moskalenko, F. C. Jones, A. W. Strong, and V. N. Zirakashvili, *Astrophys. J.* **642**, 902 (2006), astro-ph/0510335.
- [39] F. Donato, D. Maurin, P. Salati, A. Barrau, G. Boudoul, and R. Taillet, *Astrophys. J.* **563**, 172 (2001), astro-ph/0103150.
- [40] D. Maurin, R. Taillet, F. Donato, P. Salati, A. Barrau, and G. Boudoul, *ArXiv Astrophysics e-prints* (2002), astro-ph/0212111.
- [41] F. Donato, N. Fornengo, D. Maurin, P. Salati, and R. Taillet, *Phys. Rev. D* **69**, 063501 (2004), astro-ph/0306207.
- [42] A. Putze, L. Derome, and D. Maurin, *Astron. Astrophys.* **516**, A66 (2010), arXiv:1001.0551 [astro-ph.HE].
- [43] M. Cirelli, G. Corcella, A. Hektor, G. Hütsi, M. Kadastik, P. Panci, M. Raidal, F. Sala, and A. Strumia, *J. Cosmol. Astropart. Phys.* **3**, 051 (2011), arXiv:1012.4515 [hep-ph].
- [44] M. E. Wiedenbeck, N. E. Yanasak, A. C. Cummings, A. J. Davis, J. S. George, R. A. Leske, R. A. Mewaldt, E. C. Stone, P. L. Hink, M. H. Israel, M. Lijowski, E. R. Christian, and T. T. von Rosenvinge, *Space Sci. Rev.* **99**, 15 (2001).

- [45] M. E. Wiedenbeck, W. R. Binns, and A. C. Cummings, in *Proc. 30th Int. Cosmic Ray Conf. (Merida)*, Vol. 2 (2008) p. 149.
- [46] J. Goodman and J. Weare, *Communications in Applied Mathematics and Computational Science* **5**, 65 (2010).
- [47] D. Foreman-Mackey, D. W. Hogg, D. Lang, and J. Goodman, *Publications of the Astronomical Society of the Pacific* **125**, 306 (2013), arXiv:1202.3665 [astro-ph.IM].
- [48] M.-Y. Cui, Q. Yuan, Y.-L. S. Tsai, and Y.-Z. Fan, *Physical Review Letters* **118**, 191101 (2017), arXiv:1610.03840 [astro-ph.HE].
- [49] J. J. Connell, *Astrophys. J. Lett.* **501**, L59 (1998).
- [50] N. E. Yanasak, M. E. Wiedenbeck, R. A. Mewaldt, A. J. Davis, A. C. Cummings, J. S. George, R. A. Leske, E. C. Stone, E. R. Christian, T. T. von Rosenvinge, W. R. Binns, P. L. Hink, and M. H. Israel, *Astrophys. J.* **563**, 768 (2001).
- [51] A. Lukasiak, in *International Cosmic Ray Conference*, International Cosmic Ray Conference, Vol. 3 (1999) p. 41.
- [52] J. A. Simpson and M. Garcia-Munoz, *Space Sci. Rev.* **46**, 205 (1988).
- [53] T. Hams, L. M. Barbier, M. Bremerich, E. R. Christian, G. A. de Nolfo, S. Geier, H. Göbel, S. K. Gupta, M. Hof, W. Menn, R. A. Mewaldt, J. W. Mitchell, S. M. Schindler, M. Simon, and R. E. Streitmatter, *Astrophys. J.* **611**, 892 (2004).
- [54] O. Adriani, G. C. Barbarino, G. A. Bazilevskaya, R. Bellotti, M. Boezio, E. A. Bogomolov, M. Bongi, V. Bonvicini, S. Borisov, S. Bottai, A. Bruno, F. Cafagna, D. Campana, R. Carbone, P. Carlson, M. Casolino, G. Castellini, M. P. De Pascale, C. De Santis, N. De Simone, V. Di Felice, V. Formato, A. M. Galper, L. Gris-hantseva, A. V. Karelin, S. V. Koldashov, S. Koldobskiy, S. Y. Krutkov, A. N. Kvashnin, A. Leonov, V. Malakhov, L. Marcelli, A. G. Mayorov, W. Menn, V. V. Mikhailov, E. Mocchiutti, A. Monaco, N. Mori, N. Nikonov, G. Osteria, F. Palma, P. Papini, M. Pearce, P. Picozza, C. Pizzolotto, M. Ricci, S. B. Ricciarini, L. Rossetto, R. Sarkar, M. Simon, R. Sparvoli, P. Spillantini, Y. I. Stozhkov, A. Vacchi, E. Vannuccini, G. Vasilyev, S. A. Voronov, Y. T. Yurkin, J. Wu, G. Zampa, N. Zampa, V. G. Zverev, M. S. Potgieter, and E. E. Vos, *Astrophys. J.* **765**, 91 (2013), arXiv:1301.4108 [astro-ph.HE].
- [55] S.-J. Lin, X.-J. Bi, J. Feng, P.-F. Yin, and Z.-H. Yu, *ArXiv e-prints* (2016), arXiv:1612.04001 [astro-ph.HE].
- [56] H.-B. Jin, Y.-L. Wu, and Y.-F. Zhou, *ArXiv e-prints* (2017), arXiv:1701.02213 [hep-ph].
- [57] A. Cuoco, M. Krämer, and M. Korsmeier, *Phys. Rev. Lett.* **118**, 191102 (2017).
- [58] D. Maurin, F. Donato, R. Taillet, and P. Salati, *Astrophys. J.* **555**, 585 (2001), astro-ph/0101231.
- [59] D. Foreman-Mackey, *The Journal of Open Source Software* **24** (2016), 10.21105/joss.00024.
- [60] D. Maurin, F. Melot, and R. Taillet, *Astron. Astrophys.* **569**, A32 (2014), arXiv:1302.5525 [astro-ph.HE].